# The MArine Debris hyperspectral reference Library collection (MADLib)

Ashley Ohall[1], Kelsey Bisson[2], Shungudzemwoyo P. Garaba[3] and Sara Rivero-Calle[1]

[1]Skidaway Institute of Oceanography and Department of Marine Sciences, University of Georgia, 10 Ocean Science Circle, Savannah, GA 31411, USA
[2]Earth Science Division, Ocean Biology and Biogeochemistry Program, National Aeronautics and Space Administration Headquarters, Washington, DC, USA
[3]Niedersächsische Zentrum für Marine Sensorik, Carl von Ossietzky Universität Oldenburg, Schleusenstraße 1, 26382 Wilhelmshaven, Germany

*Correspondence to*: Sara Rivero-Calle (rivero@uga.edu)

**Abstract.** Marine debris is a ubiquitous and growing threat to environmental and human health. Efforts to monitor and mitigate marine debris pollution face many challenges. The absence of standardized methodologies is a primary limitation for monitoring capabilities due to the complex and diverse physical and chemical properties of marine debris. Variabilities include object size, apparent color, polymer type, weathering, and aqueous state. Despite the challenges in object characteristics, advances in remote sensing methods show promise for detecting marine debris across local to global scales. Algorithms are needed to link remotely sensed observations with relevant characteristics of marine debris to fully realize this potential. Although more optical measurements of marine debris reflectance are becoming available for algorithm development, inconsistencies in data curation remains an obstacle. Variations in data processing and inconsistent metadata hinder efforts to develop robust, generalizable algorithms for marine debris detection. To address this, we present the well-curated MArine Debris hyperspectral reference Library collection (MADLib) containing 24889 reflectance spectra from 3032 samples. All optical measurements are available in open access via https://doi.org/10.4121/059551d3-2383-4e20-af2d-011c9a59d3ac (Ohall et al., 2025). MADLib demonstrates the importance of open-science and open-access datasets, as it compiles and harmonizes spectral data collected from publicly accessible datasets and individual research projects. Consistent methods were applied for data standardization, quality assurance, and integration. We also propose a robust protocol for generating metadata tailored to marine debris and ocean color remote sensing applications. MADLib possesses spectra of a wide range of marine debris materials including different polymer types, color, size, weathering, and aqueous states. Here, we analyze the metadata associated with the spectra to identify sampling gaps and propose considerations for future work. By providing open-access and standardized data, MADLib is expected to support the development of robust marine debris detection algorithms.

**Keywords**: Marine debris; Marine litter; Hyperspectral reflectance library; Plastics; Polymer.

## 1. Introduction

Marine debris or litter is any persistent solid material that is manufactured or processed and directly or indirectly disposed of or abandoned in an aquatic environment (Cheshire et al., 2009). Marine debris has become ubiquitous across all aquatic environments due to the rapid production of manufactured goods without proper disposal management (UNEP, 2021; Thompson et al., 2024; Galgani et al., 2025). The negative implications of mismanaged marine debris on blue economic activities, environmental and human health are extensive, prompting a need for effective monitoring and tracking to support informed mitigation strategies (Beaumont et al., 2019; Smith and Garaba, 2025; GIZ, 2023; NASEM, 2021).

Remote sensing has the potential to support the monitoring of aquatic debris concentrations and dispersal patterns across spatial and temporal scales. From this perspective, the definition of marine debris is broadened to include not only anthropogenic materials, but also natural materials such as algal patches, wood, pollen, pumice or seaweed species (Martínez-Vicente et al., 2019; Maximenko et al., 2019; NASEM, 2021; Hu et al., 2023; Garaba et al., 2023). However, ongoing efforts in remote sensing of marine debris are challenging due to the complexity of the targets (de Vries et al., 2023a; NASEM, 2021; GIZ, 2023). Debris objects vary widely in physical properties (e.g., color, shape, composition, size) that are further influenced by environmental factors such as aqueous state and stage of weathering
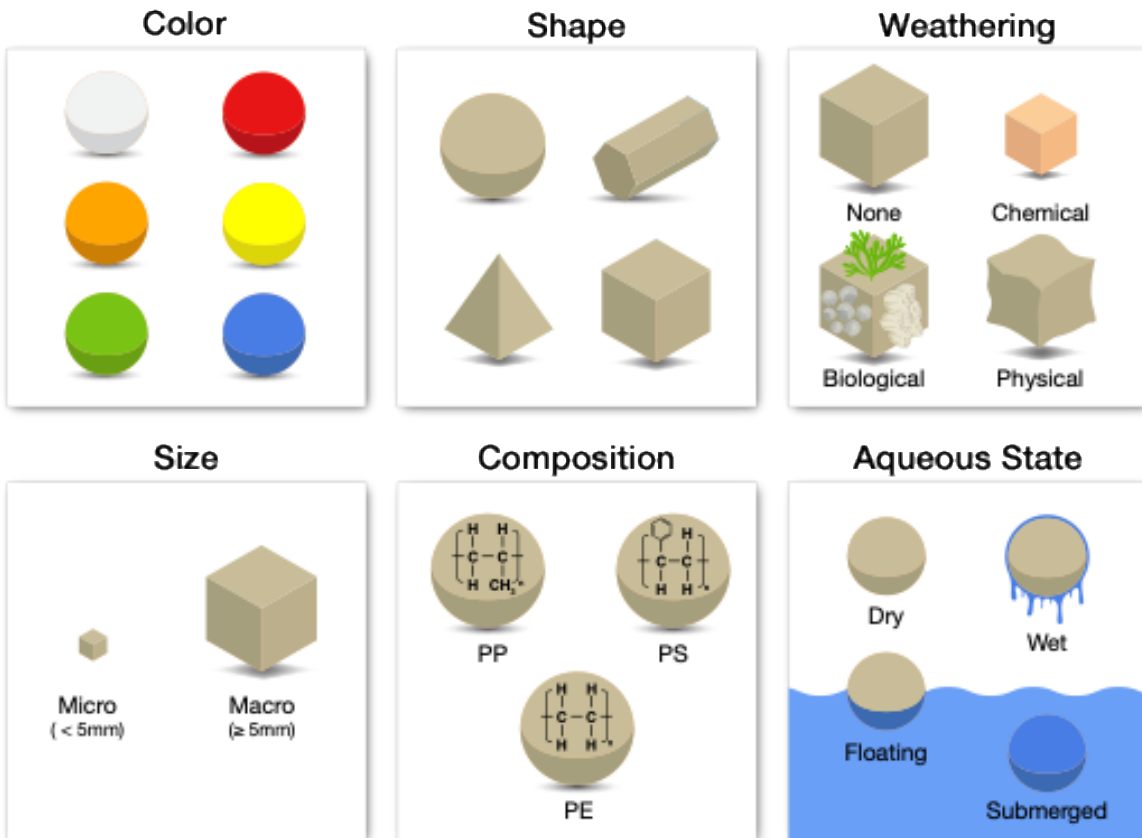
**Figure 1. Examples of physical and chemical characteristics of marine debris in nature.**

50 (**Figure 1**). Fully understanding marine debris diagnostic optical properties is essential for building, training, and
51 validating remote sensing detection algorithms (Garaba et al., 2021a; Garaba and Harmel, 2022). This information,
52 together with the evolution of hyperspectral remote sensing technologies and the development of active and passive
53 sensors, is expected to further advance current capabilities to detect and monitor marine debris.

54 The reflectance parameter is one of the common remote sensing parameters that describes the ratio of light reflected
55 off an optically active sample with respect to a known standard like a Lambertian equivalent target. Reflectance
56 measurements, when collected under controlled conditions using instruments such as handheld spectroradiometers,
57 minimize the environmental variability, which is ideal for initial algorithm development (Knaeps et al., 2021; de Vries
58 et al., 2023a; Garaba et al., 2021a; Garaba et al., 2020a). Recent stakeholder discussions facilitated by the International
59 Ocean Color Coordinating Group Task Force on Remote Sensing of Marine Litter and Debris highlighted the need
60 for a comprehensive, well-curated spectral reference library (SRL) of marine debris reflectance. SRLs support
61 algorithm development by offering spectral data of known objects, establishing a baseline database that can be used
62 to identify unknown objects. However, current marine debris reflectance datasets have been gathered using variable
63 methodologies, data processing, and metadata curation, making it challenging to combine them for algorithm
64 development and to identify gaps in the field.

65 In this study, we leverage the wealth of available spectral reflectance measurements of marine debris to build a
66 consistent and extensive collection. We compiled, assessed and curated the available marine debris reflectance datasets
67 into a single SRL called the MArine Debris hyperspectral reference Library collection (MADLib). MADLib aims to
68 improve the accessibility and comparability of current data to promote the spectral exploration and analysis needed
69 for marine debris algorithm development. We also aimed to follow the FAIR guidelines by making the data findable,
70 accessible, interoperable, and reusable (Wilkinson et al., 2016). Here, we explain how the data contained in the
71 collection was curated, identify existing sampling gaps, and discuss factors that are important for the trustworthiness
72 of future SRLs and remote sensing of marine debris.

73 **2. Methods and materials**

74 **2.1 Selection of datasets**

75 Thirteen datasets were selected for curation and creation of MADLib collection from open-access sources as well as
76 upon request from authors (**Table 1**). The selected datasets have the following characteristics (i) the data reported
77 were relative reflectance not remote sensing reflectance, (ii) reflectance was measured using a handheld
78 spectroradiometer, and (iii) hyperspectral data were provided in the visible to Shortwave Infrared (SWIR) region. The
79 remaining datasets found in the literature either did not meet these criteria, were not readily available upon request, or
80 needed further curation from the authors e.g., (Acuña-Ruz and Mattar, 2020; Olyaei et al., 2024; Tasseron et al., 2021;
81 Wang et al., 2024; Knaeps et al., 2020). Leveraging the datasets (**Table 1**), we determined a standard formatting
82 structure from which to build the MADLib collection. This included several spectral data processing steps for quality
83 control (**Section 2.3**) and gathering additional metadata parameters about the samples (**Section 2.4**).

84    **Table 1. Source of hyperspectral measurements used to create MADLib.**

| Dataset Number | Reference | Data access | Number of samples | Keywords |
|---|---|---|---|---|
| 1 | (Corbari et al., 2020) | Author Permission | 65 | Dry, Floating, Pristine, Micro, Varying Thickness, Varying Pixel Coverage |
| 2 | (de Vries and Garaba, 2023) | CC BY 4.0 | 575 | Dry, Wet, Submerged, Pristine, Naturally Weathered |
| 3 | (de Vries et al., 2023b) | CC BY 4.0 | 115 | Dry, Submerged, Lab Weathered |
| 4 | (English and Hu, 2020) | ODC BY 1.0 | 6 | Dry, Floating, Pristine, Naturally Weathered |
| 5 | (Garaba et al., 2021a) | CC BY 4.0 | 793 | Dry, Floating, Pristine, Naturally Weathered, Varying Pixel Coverage |
| 6 | (Garaba et al., 2020b) | CC BY 4.0 | 80 | Dry, Wet, Submerged, Pristine, TSM |
| 7 | (Garaba and Dierssen, 2017) | CC BY 4.0 | 11 | Dry, Pristine, Micro |
| 8 | (Garaba and Dierssen, 2019c) | CC BY 4.0 | 2 | Dry, Wet, Naturally Weathered, Micro |
| 9 | (Garaba and Dierssen, 2019a) | CC BY 4.0 | 6 | Dry, Naturally Weathered, Micro (specific size classes) |
| 10 | (Garaba and Dierssen, 2019b) | CC BY 4.0 | 23 | Dry, Naturally Weathered, Macro |
| 11 | (Garaba et al., 2021b) | CC BY 4.0 | 9 | Dry, Floating, Naturally Weathered, Pristine |
| 12 | (Leone et al., 2021) | CC BY 4.0 | 1077 | Dry, Wet, Submerged, Pristine, Lab Weathered, Naturally Weathered, TSM, Algae |
| 13 | (Corbari et al., 2024) | Author Permission | 270 | Naturally Weathered, Black Background vs White Background |

85

86    **2.2 Materials**

87    MADLib includes 3032 samples compiled from thirteen datasets (**Table 1**). Each sample represents either a single

88    marine debris object (e.g., a bottle, buoy) or an assemblage of micro-sized items (e.g., a collection of microplastic

89    particles measured together) measured under specific conditions. For example, the same object measured in both dry

and submerged states was represented as two separate samples in MADLib. Each sample is associated with a spectrum and the related metadata. The samples encompass a wide variety of colors, sizes, polymer types, weathering conditions, aqueous states, and experimental designs. It should be noted that, while these datasets include various debris types, plastic is the dominating type of debris reported, reflecting its overwhelming presence in the marine environment.

## 2.3 Spectral data processing

Each dataset was downloaded from its respective open-access platform or requested from the corresponding author and assembled into MADLib. Spectral reflectance measurements covered a wavelength range between 280-2500 nm with 1 nm resolution. In most cases, multiple spectral measurements were recorded per sample, sometimes in various geometric orientations. We will refer to these measurements as replicates, which account for within-sample variability and instrument noise.

The final MADLib spectral data download includes five identification columns: *dataset number, sample number, data type, replicates* and *flags*. *Dataset number* refers to the cited datasets (**Table 1**). *Sample number* uniquely identifies each sample within a specific dataset. *Data type* specifies whether the data in that row represents the "mean", "median", or standard deviation "stdev" of that sample's replicates, or "single" for single measurements without replicates. *Replicates* provides the number of replicates associated with that statistical representation. The *Flags* column contains a "1" to spectra containing more than 50 % NaN values and otherwise contains a "0". The data are sorted alphanumerically by *data type*, then *dataset number,* and finally *sample number*.

### 2.3.1 Data formatting

Spectral data were obtained in one of four formats depending on the dataset: (1) individual spectral measurements for each replicate, (2) pre-calculated means, medians, and standard deviations of the replicates per sample, (3) only the mean spectral reflectance values of the replicates per sample, or (4) single reflectance measurements per sample without replicates.

When more than one individual spectral measurement per sample was provided, the mean, median, and standard deviation of the replicate measurements were calculated for each sample to standardize across datasets. Two datasets provided only mean spectral reflectance values of their sample's replicate measurements, so the median and standard deviation for these data were written as NaNs (Not a Number) in MADLib. Single measurements were provided for six samples across three datasets and were classified separately as "single".

MADLib only reports the descriptive statistics of the compiled data as mean, median and standard deviation of the replicates (with the two exceptions specified above). In total, MADLib summarizes the information from 24889 replicate measurements of 3032 samples collected from thirteen datasets (**Figure 2**). In the datasheet, 3026 mean measurements, 2691 median measurements, and 2691 standard deviation measurements are recorded. Six samples did not have replicates, so they are available as individual measurements without summary statistics.
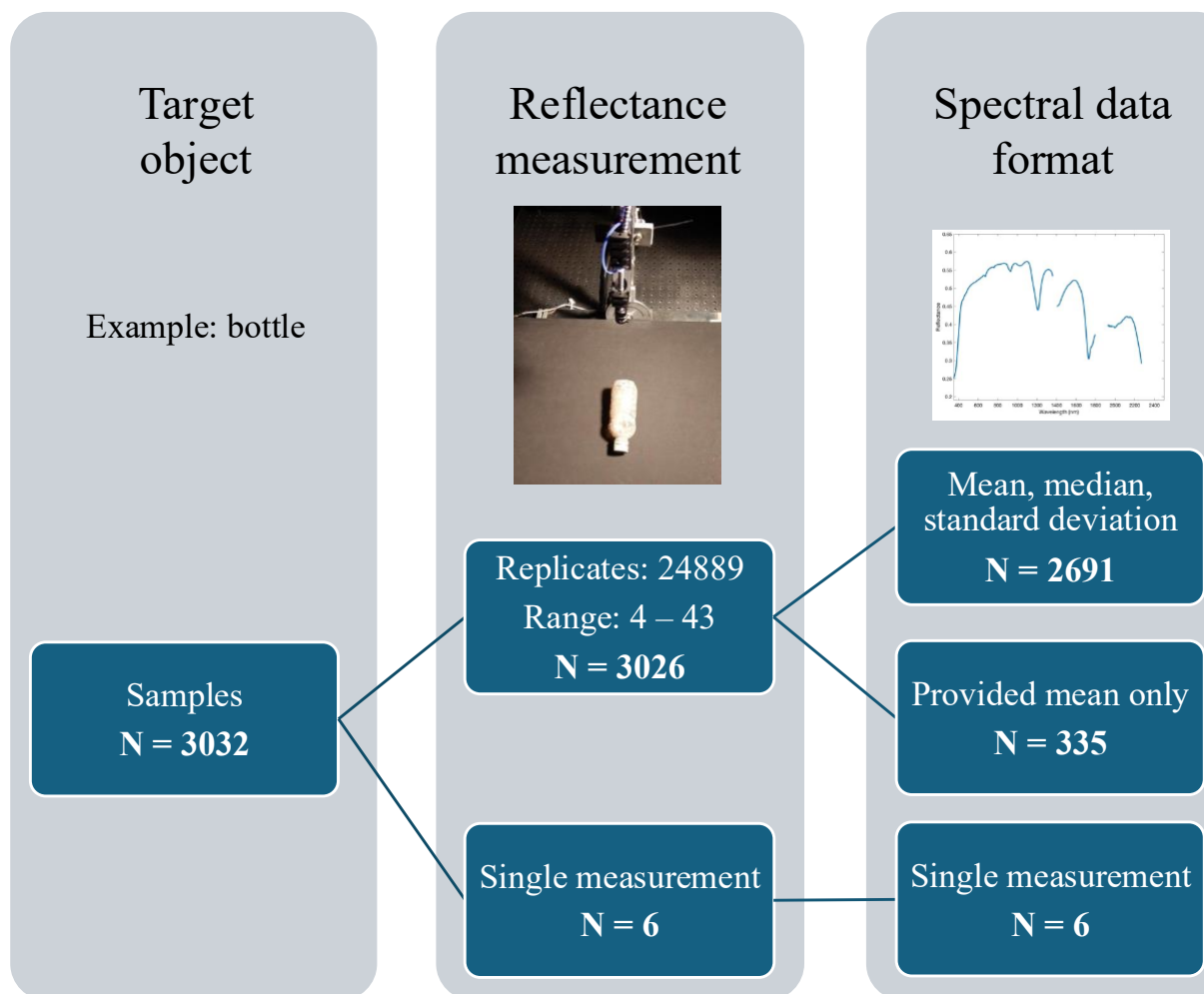
**Figure 2. Breakdown of the number of samples, replicate measurements for total samples, and descriptive statistics of sample spectra within MADLib.**

123

124 **2.3.2 Wavelength range adjustment**

125 A wavelength range limit of 280-2500 nm was applied to ensure consistency across datasets. NaNs were used in place
126 of the missing spectral data for instruments not collecting data in the fixed range.

127 **2.3.3 Splice correction**

128 Hyperspectral instruments measuring beyond the visible-near-infrared (VNIR, 280-1000 nm) consist of multiple
129 detectors, each covering a distinct spectral range. Off-the-shelf spectroradiometers commonly used in environmental
130 remote sensing applications (e.g., Analytical Spectral Devices FieldSpec 4, Spectral Evolution SR-3501, Spectral
131 Evolution SR-1901) have three detectors. When transitioning between the detectors, slight differences in sensitivity,
132 temperature or calibration can create discontinuities in the reflectance spectral measurements. The spectral
133 discontinuities, or "steps", usually occur around 1000-1001 nm and 1800-1801 nm, but the exact positions are

instrument and manufacturer specific (**Figure 3a**). The spectral data from each dataset were visually inspected for steps. If a step was identified, we calculated the linear difference at each step and adjusted one region of the spectrum based on another to eliminate the gap (Garaba et al., 2021a). The middle detector (1000-1800 nm) was considered as the reference, and the adjacent regions (280-1000 nm and 1800-2500 nm) were adjusted to that reference level. For example, if the reflectance difference between 1000 nm and 1001 nm is -0.02, then 0.02 is subtracted from all values in the 280-1000 nm range to align it with the more stable middle region (**Figure 3b**).
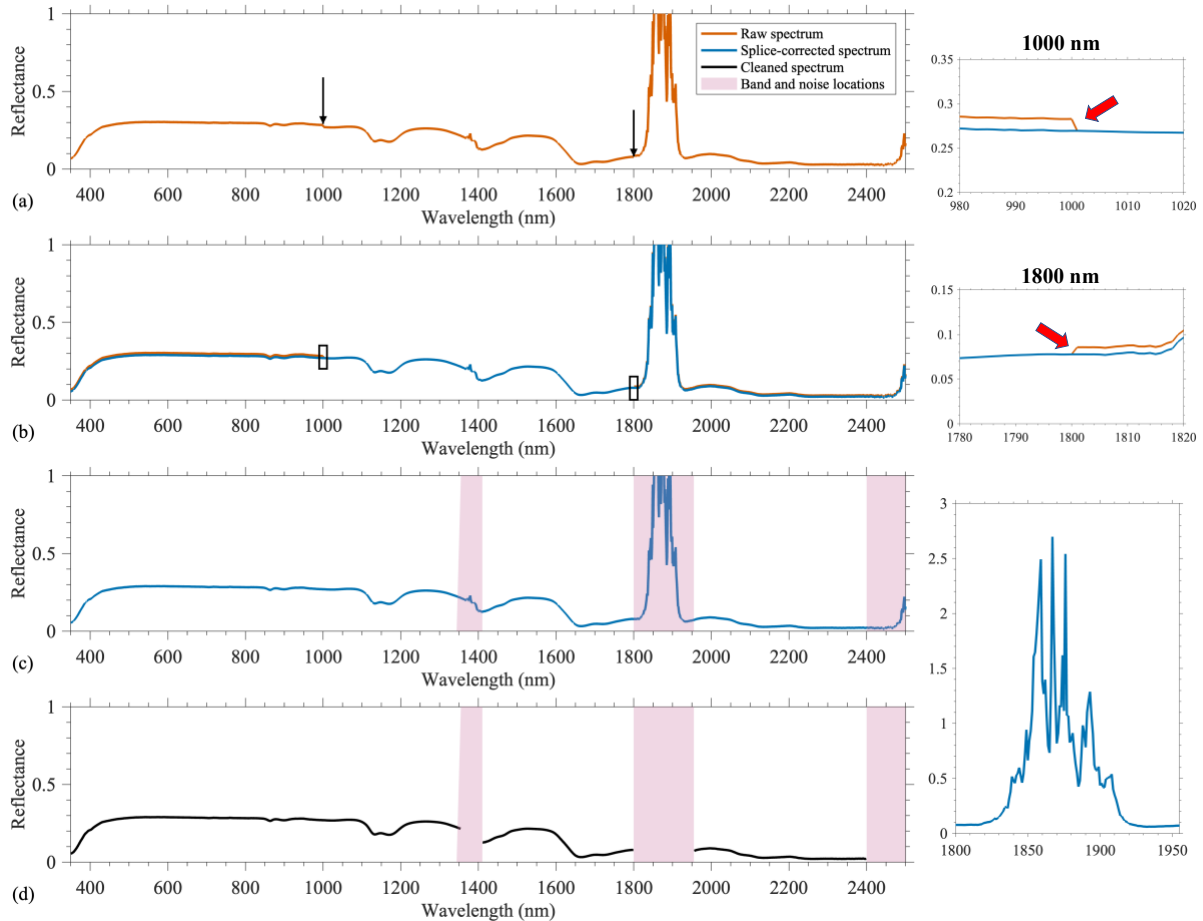
**Figure 3. Example processing steps for spectra: (a) raw downloaded spectrum; (b) comparison of raw and splice-corrected spectra, (c) identification of atmospheric absorption bands and instrument noise; and (d) final cleaned spectrum. Zoom-in boxes show the 980–1020 nm and 1780–1820 nm regions in (b), highlighting the steps and splice correction at 1000 nm and 1800 nm, and the 1800-1950 nm region in (d), highlighting the full reflectance magnitude of the atmospheric absorption band.**

### 2.3.4 Noise removal

Visual inspection was used to identify, and subsequently remove, noise in the spectra. The affected wavelengths were replaced with NaNs to avoid misinterpreting them as real spectral features in later analyses (**Figure 3d**). Noise was considered to arise from two main sources: atmospheric absorption bands and instrument-related noise. Strong

atmospheric absorption occurs in the SWIR, specifically around 1350–1450 nm, 1800–1950 nm, and above 2400 nm (Garaba and Dierssen, 2020; Clark et al., 2003). This effect is observed in outdoor measurements, where sunlight interacts with larger portions of the atmosphere before reaching the sample. Spectra often exhibit abrupt, isolated peaks due to these atmospheric absorption bands. Instrument noise was also observed, particularly at the extreme ends of the spectral range, where sensor sensitivity tends to decrease.

### 2.3.5 Flags

Hyperspectral data (mean, median, standard deviation, or single measurement) with more than 50 % NaN values across the original wavelength range were flagged. The flagged entries were kept in MADLib for completeness but were marked with an additional *flags* column to indicate data quality. A binary code of "1" indicates a flagged sample, while "0" indicates a clean sample.

### 2.4 Metadata curation

MADLib incorporates the unique metadata provided for samples from each dataset, adds new metadata parameters, and ultimately provides comprehensive metadata descriptors for improved interoperability. Metadata descriptors date/time, longitude, latitude, FTIR identification, and sample weight were excluded from the curation due to their limited applicability across datasets and the potential for misleading interpretation since the samples were not imaged in situ. Metadata were incorporated from existing metadata files, descriptions within associated publications, and, when necessary, missing details were obtained from the authors directly. When this was not possible, NaN values were assigned to indicate the missing metadata. The final MADLib metadata download includes thirty-nine columns of metadata descriptors **(Table 2)**. The thorough curation process in MADLib enabled more detailed and robust analyses, focusing on parameters that enhance the identification and classification of marine debris through reflectance measurements.

**Table 2. List of MADLib metadata descriptors.**

| Meta column name | Description |
|---|---|
| DatasetNumber | Unique library identifier |
| SampleNumber | Unique sample identifier |
| Polymer Type | Standard abbreviation for plastic polymer (**Table 3**) |
| Object Type | Purpose or use of object |
| Object State | Describes how an object was physically altered or interacted with |
| Origin | Manufacturer or location sample was collected |

| | |
|---|---|
| White / Transparent / Red / Orange / Yellow / Green / Blue / Purple / Brown / Gray / Black / Multi | Binary indicator for the apparent color of sample: present (1) or absent (0) |
| Length | First dimension provided (mm) |
| Width | The second dimension provided, if applicable (mm) |
| Height | The third dimension provided, if applicable, or sample thickness (mm) |
| Categorical Size | Micro or macro |
| Weathering State | Pristine, lab weathered, or naturally weathered |
| Laboratory Weathering Type | If lab weathered: phytoplankton/biofilm, UV degradation, or other |
| Aqueous State | Dry, wet, submerged, or floating |
| Submergence Depth | Sample depth below water surface (mm) |
| Water Type | Freshwater, saltwater, seawater, artificial seawater, or filtered seawater |
| TSM | Total suspended matter concentration (mg/L) |
| Algal Cell Density | Number of microalgae cells per milliliter of water (cells/mL) |
| Pixel Coverage | Proportion of instrument field of view covered by an object (%) |
| Glass Presence | G = glass held sample in place, N = no glass, NaN = not applicable |
| Setting | Indoors or outdoors |
| Instrument | Manufacturer or brand name of spectroradiometer |
| Lighting | Artificial or ambient natural light source |
| Background | Black background, white background, concrete, land, water |
| Reference Standard | Reference plaque reflectance percentage |
| Fixed Height from Sample | Distance from fore optic to object surface (dry, wet) or water surface (submerged, floating) (m) |
| FoV | Field of view of the bare fiber optic or fore optic lens (deg) |

| Viewing Geometry | Nadir viewing angle (deg) |
|---|---|

167

### 2.4.1 Sample type

169 Despite MADLib containing a variety of marine debris types, it is primarily composed of plastic debris. Consequently,
170 this paper will address plastic-specific characteristics, such as polymer type, in addition to broader characteristics.
171 Sample type parameters included *polymer type*, *object type*, *object state,* and *origin* to maximize dataset comparability.
172 For example, if a dataset described a sample as "crushed PET water bottle", we further described it using *polymer type*
173 = "PET", *object type* = "bottle", and *object state* = "crushed". During this process, the *polymer type, object type*, and
174 *object state* were simplified or modified to ensure consistency and comparability across datasets. For example, object
175 types labeled as "water bottle", "clear water bottle", "bottle", "plastic bottle", or any similar terminology were all
176 simplified to "bottle". *Origin* was provided if the dataset specified the manufacturer or place the item was retrieved
177 from.

### 2.4.2 Color

179 Colors are categorized as *white, transparent, red, orange, yellow, green, blue, purple, brown, gray, black,* and *multi*
180 to ensure consistency and comparability across samples. For example, pre-existing samples marked as tan, dark brown,
181 light brown, and brown were all included in the *brown* category. Colors were recorded with binary entries to easily
182 identify objects with multiple colors. If more than one color was specified by the original author, all relevant colors
183 were marked with a 1. If multi-colored was specified by the original author, only *multi* was marked with a 1.

### 2.4.3 Size

185 Object dimensions were recorded differently across datasets and required representation in various formats. The
186 *length, width,* and *height* columns were used for objects with complete dimensional data, while the *height* column
187 additionally represented thickness where relevant. If a range of sizes was provided (e.g., 1-3 mm) by the authors of
188 the original dataset, then the average was included (e.g., 2 mm) in MADLib. If a height or thickness of <1 mm was
189 provided, then 1 mm was reported. In some cases, the authors alternatively provided categorical size data, either
190 "micro" (<5 mm) or "macro" (>5 mm), so we included a *categorical size* classification. Samples with numerical data
191 provided were categorized as "micro" if all three dimensions (L, W, H) were <5 mm. If only partial size data were
192 available and under 5 mm, samples were not categorized as "micro" to avoid errors in cases where a missing dimension
193 might exceed 5 mm. Conversely, any sample with one or more dimensions >5 mm was classified as "macro".

### 2.4.4 Weathering

195 *Weathering state* was specified as either "pristine", indicating non-weathered, virgin material; "lab weathered",
196 subjected to controlled laboratory conditions; or "naturally weathered", collected from the marine environment and

exposed to natural processes. The specific type of lab weathering was indicated as either "biofouled" or "UV exposure" in the *lab weathering type* metadata column. Samples labeled as "biofouled" were submerged in natural water within a mesocosm to promote biofilm growth (de Vries et al., 2023b; Leone et al., 2021). Some of these samples were additionally labeled as rough if their surfaces had been abraded with sandpaper prior to submersion (Leone et al., 2023). To simulate photodegradation, other samples were exposed to ultraviolet (UV) radiation under either dry or wet conditions (Leone et al., 2023).

**2.4.5 Aqueous state and water properties**

Four categories describe the a*queous state* of the samples: "dry", "floating", "submerged", and "wet". "Dry" samples refer to dry objects measured on a dry surface. "Wet" samples refer to wet objects measured on a dry surface or above a water body. "Floating" samples refer to any object floating on the surface of a water body or in a water tank. "Submerged" samples refer to any object where the top is at least 1 mm under the water's surface.

If the sample was categorized as "wet", "floating", or "submerged", and information on the properties of the water in which it was measured were available, they were also included. *Water type* specifies if the sample was measured in "freshwater", "saltwater", "seawater" (unfiltered), "artificial seawater", or "filtered seawater". In some cases, samples were measured in a mesocosm or water bath that had added total suspended matter (TSM) or phytoplankton (Leone et al., 2021; Garaba et al., 2020b). Concentrations were included in *TSM* and *algal cell density* columns. Additionally, the submergence depth of samples in millimeters under the water surface was provided in the *submergence depth (mm)* column, ranging from 5-715 mm.

**2.4.6 Experimental setup**

The location of measurement, *setting*, was categorized as "indoors" or "outdoors" for all samples. *Lighting* was similarly categorized for each location, with indoors using tungsten halogen lamps, or outdoors using sunlight with recorded conditions (**Figure 4**). Studies also varied with the *viewing geometry, field of view (FoV)*, and *fixed height from sample*. Dry surface and water bath samples were measured on a black background with the exception of one dataset which used both black and white backgrounds for comparison (Corbari et al., 2024).

Other controlled sample parameters included *Pixel Coverage* and *Glass Presence. Pixel Coverage,* also referred to as areal fractional cover, refers to the percentage of the field of view containing the sample and was used to measure varying concentrations of microplastics (Garaba et al., 2021a; Corbari et al., 2020). Glass was used in one dataset to hold samples in place, therefore causing a possible disruption to the produced spectra (de Vries and Garaba, 2023). Further information on protocols specific to each dataset may be found in the original publications (Corbari et al., 2024; Corbari et al., 2020; de Vries et al., 2023a; English and Hu, 2020; Garaba and Dierssen, 2020; Knaeps et al., 2021; Garaba et al., 2021a; Garaba et al., 2021b; Leone et al., 2023).
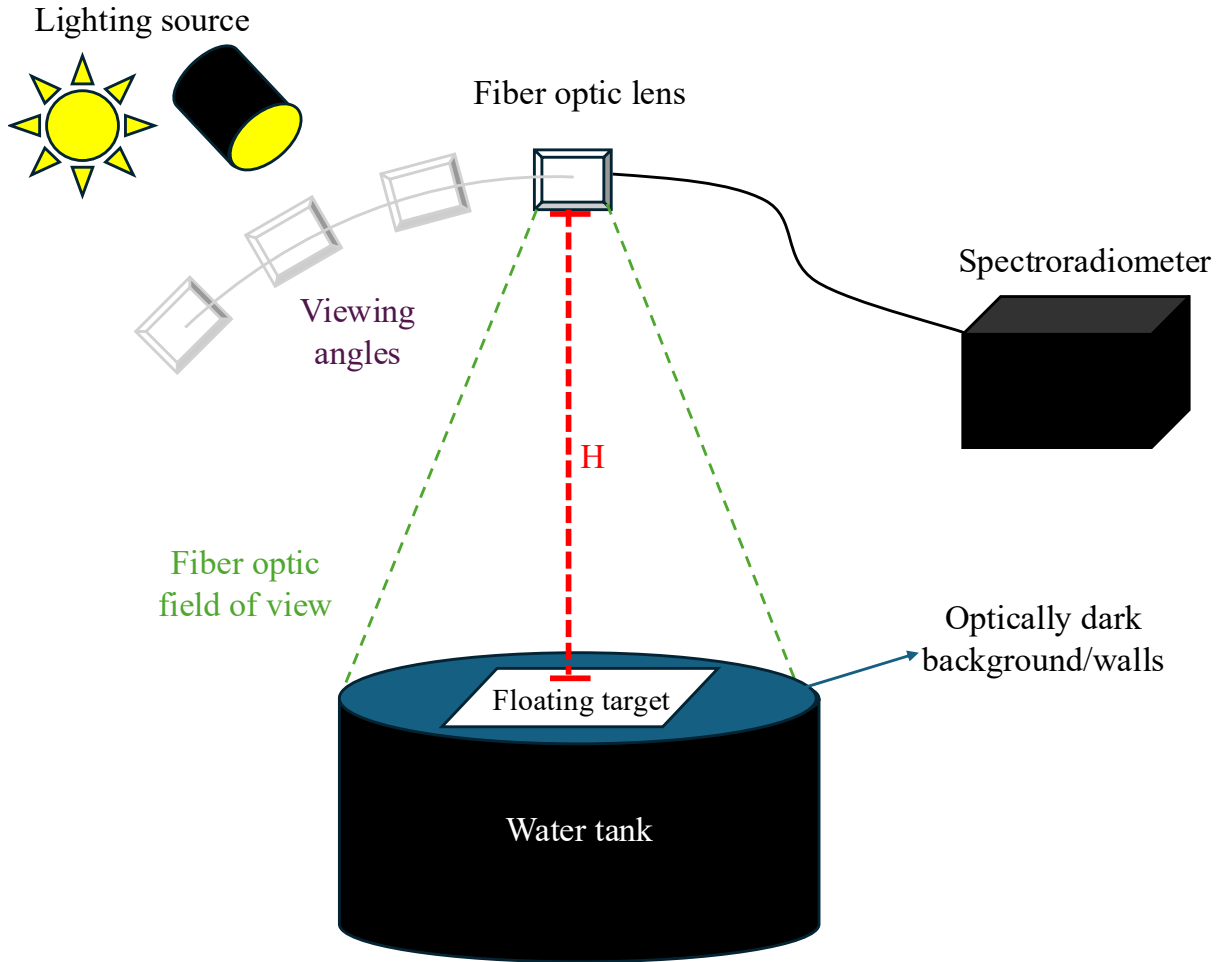
**Figure 4. Schematic of typical experimental setup with the light source, variable viewing geometry, fiber optic field of view, fixed height from sample (H), and an optically dark background.**

228

229 **3. Results**

230 Here, we examine the distributions of several characteristics within MADLib and present case studies of spectral

231 reflectance where relevant. To ensure consistency, all spectra plotted in this study correspond to the mean of replicate

232 measurements for each sample.

233 **3.1 Polymer type**

234 Nineteen distinct polymer types are included in the dataset (**Table 3**). The largest group of samples are of an unknown

235 polymer type (35 %) (**Figure 5a**). The unknown polymer category includes plastics with unidentified polymer types

236 as well as non-plastic marine debris, such as fabrics, metals, and background materials. Polypropylene (PP) is the

237 most common polymer type, making up 15 % of the samples, followed by polystyrene (PS) and high-density

238 polyethylene (HDPE) (**Figure 5a**). Only one sample is available for each of the following six polymers: terpolymer

239 lustran 752 (ABS), fluorinated ethylene propylene teflon (FEP), merlon, polyamide 6.6 (PA6.6), polymethyl

240 methacrylate (PMMA) and thermoplastic elastomer (TPE). Some polymer types in MADLib exhibit similar spectral

241 features across the NIR–SWIR range, while others display distinct or minimal spectral features (**Figure 5b**).

242 The reflectance spectra of all pristine, dry PP and HDPE samples are isolated and presented separately to inspect intra-

243 variability in spectral features of measured polymers (**Figure 5c, d**). These polymers were selected because they are

244 well represented in MADLib, with numerous samples originating from several independent datasets. The spectral

245 shape in the visible spectrum is consistent with the apparent color of each object; this is further explored in **Section**

246 **3.3**. In the case of the PP samples, the objects in dataset 6 were observed to be transparent, orange, and blue in color,

247 while those in datasets 1 and 7 were white/transparent, those in dataset 2 were grey, and those in dataset 5 were yellow

248 and brown (**Figure 5d**). Dataset 12 did not provide information on apparent color. The absorption features within the

249 SWIR are consistent across samples of the same polymer type and align closely with reported literature (Olyaei et al.,

250 2024; Garaba and Dierssen, 2020). The observed differences in magnitude between spectra from a single dataset are

251 associated with changes in sample thickness and size (datasets 1,2, and 12), glass presence (dataset 2), or pixel

252 coverage (dataset 5). Measurements between datasets also differed in acquisition, such as fiber optic field of view and

253 height of instrument from sample at time of measurement, which may affect pixel coverage.

254 **Table 3. Standard abbreviations of polymer types in MADLib.**

| Abbreviation | Polymer |
|---|---|
| ABS | Acrylonitrile butadiene styrene (lustran 752) |
| EVA | Ethylene vinyl acetate |
| FEP | Fluorinated ethylene propylene teflon |
| HDPE | High-density polyethylene |
| HDPE_LDPE | A combination of high and low-density polyethylene |
| LDPE | Low-density polyethylene |
| Merlon | Merlon |
| PA6 | Polyamide 6 (nylon 6) |
| PA6.6 | Polyamide 6.6 (nylon 6.6) |
| PE | Polyethylene |
| PET | Polyethylene terephthalate |

| | |
|---|---|
| PETa | Polyethylene terephthalate - amorphous |
| PETc | Polyethylene terephthalate - crystalline |
| PMMA | Polymethyl methacrylate |
| PP | Polypropylene |
| PS | Polystyrene |
| PS-XT | Extruded polystyrene |
| PVC | Polyvinyl chloride |
| TPE | Thermoplastic elastomer |
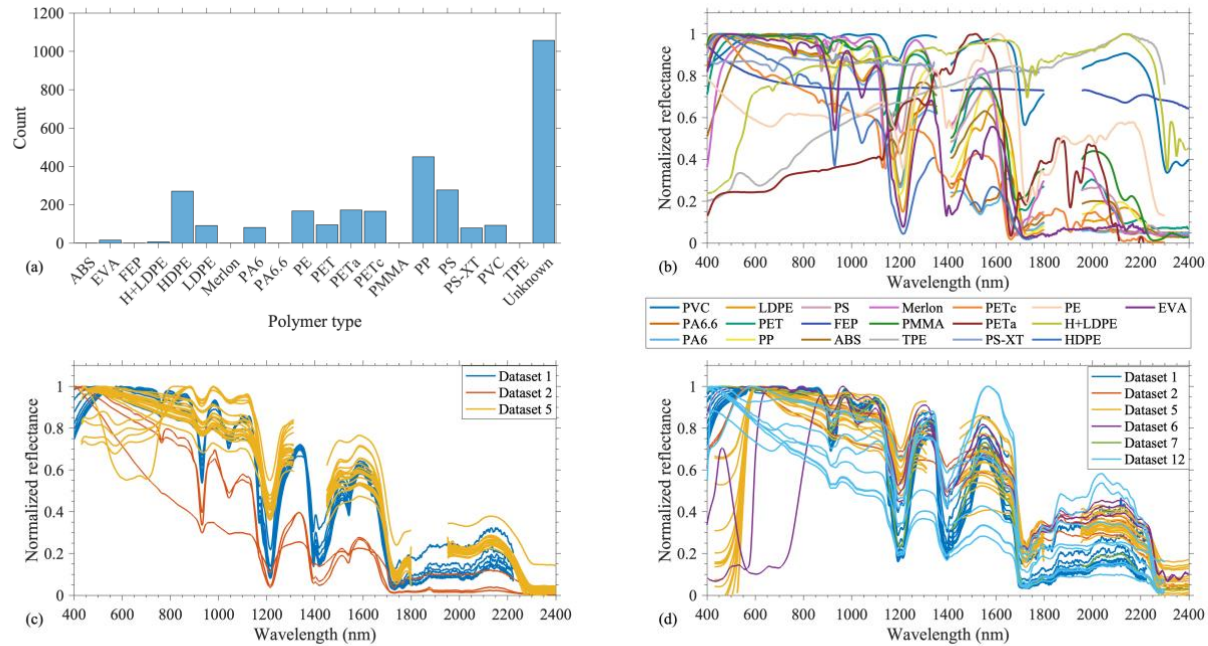
**Figure 5. (a) Distribution of polymer types; (b) example reflectance spectra for each polymer type in MADLib; (c) reflectance spectra of all available pristine, dry HDPE samples; and (d) reflectance spectra of all available pristine, dry PP samples. Each reflectance spectrum was normalized to its own maximum reflectance value.**

255

256  **3.2 Object type**

257  Thirty-nine object types are used to define the samples, noting that 17 % of samples are of unknown object type

258  (**Figure 6**). Among those that could be classified, the top two categories are sheet (33 %) and manufactured plate (16

259  %). We note that the majority (88 %) of samples labeled as sheet and all samples labeled as manufactured plate were

260  obtained directly from the manufacturer as a single polymer composition. There are five object types (bubble wrap,

261  cloth, lid, sweater, and tire) for which only one sample was measured.
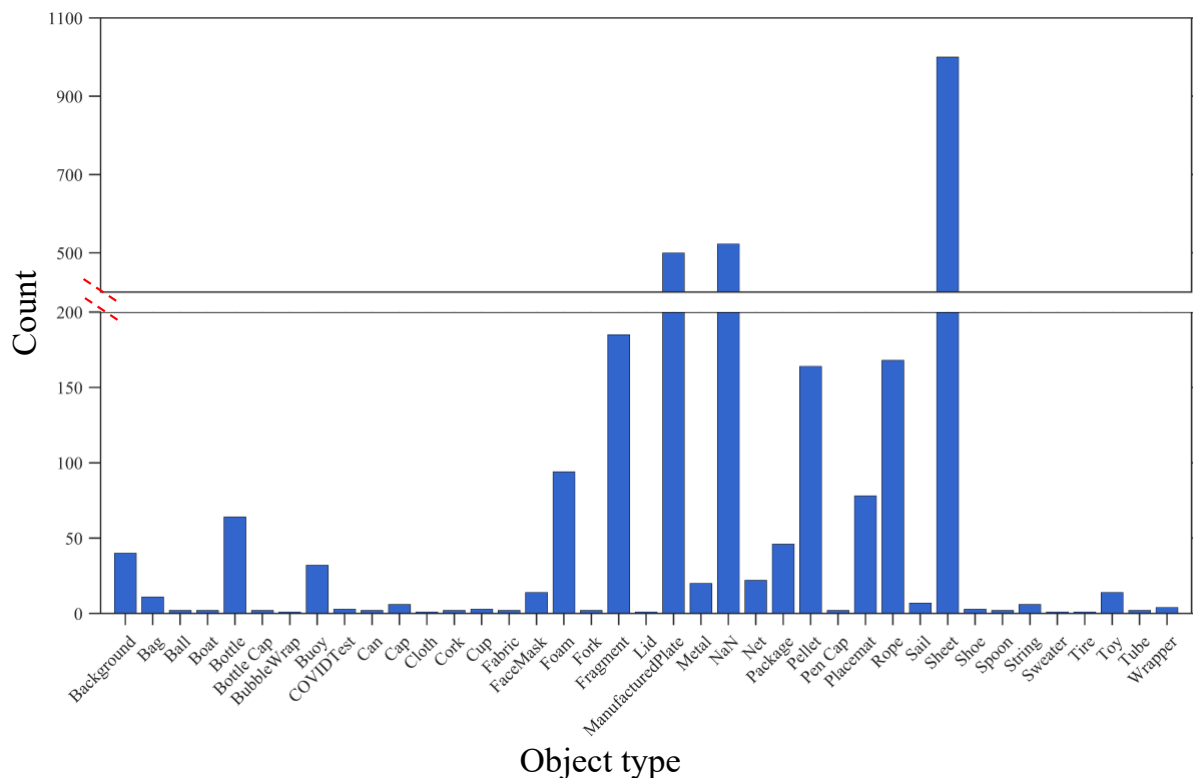
**Figure 6. Distribution of object types among samples in MADLib.**

### 3.3 Color

Twelve color categories are used in MADLib. The three largest categories are unspecified (30 %), white (19 %), and grey (15 %) (**Figure 7a**). The categories brown, black, blue, and transparent contain approximately 5-8 % of the total samples each. 16 % of the samples are categorized as having more than one color.

As expected, when color is isolated as the only changing characteristic, it most significantly influences the visible region of the spectrum (400–700 nm). For instance, blue-colored objects exhibit a reflectance peak near 470 nm, while white-colored objects show consistently high reflectance across the visible range (**Figure 7b**). In the NIR–SWIR region, absorption features associated with polymer type remain unchanged regardless of color. When different polymer types of the same color are compared, similar peaks exist in the visible region, as expected, with some minor variations (**Figure 7c- d**).
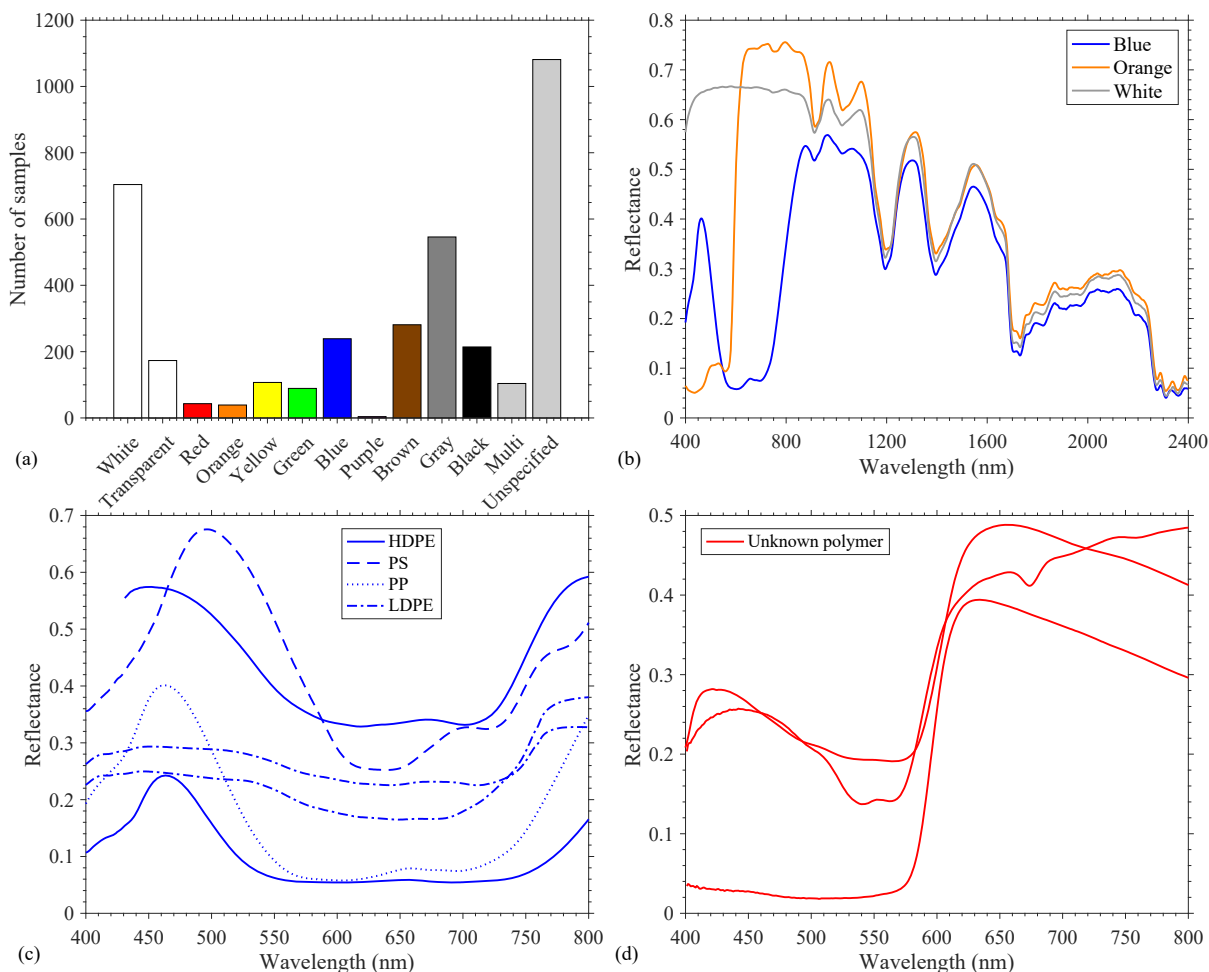
**Figure 7. (a) Distribution of sample colors within MADLib, (b) reflectance spectra of the same polymer and object (polypropylene placemat) in three different colors (c) six blue colored samples of different polymer types, and (d) three red samples of unknown polymer type.**

273

274 **3.4 Size**

275 Using the available quantitative and qualitative size data, all samples are categorized as macro, micro or uncategorized

276 due to a lack of available size data. Nearly half *(*41 %) of the samples within the dataset are unable to be categorized

277 (**Figure 8a)**. Of those categorized, the majority (90 %) are considered macro-sized, and only 10 % are micro-sized.

278 Our results show that the locations of absorption features within the SWIR are consistent for micro- and macro-sized

279 debris of the same polymer types (**Figure 8b-d**). In each example, the microplastic and macro-plastic measurements

280 are from different datasets (**Figure 8b-d**). Therefore, there are differences in sample color as well as experimental

281 setup (such as field of view or height of spectroradiometer from sample) between the two samples. Differences in

282 spectral features within the visible region are likely due to color inferred from the corresponding peaks and shapes.

283 Other slight differences in feature location may be attributed to other metadata (e.g. additives, state of weathering,

284 etc.). Additionally, we note that the HDPE microplastic spectrum has a pixel coverage of 90%, compared to 100% for

285 all other spectra.

(a)

(b)

(c)

(d)
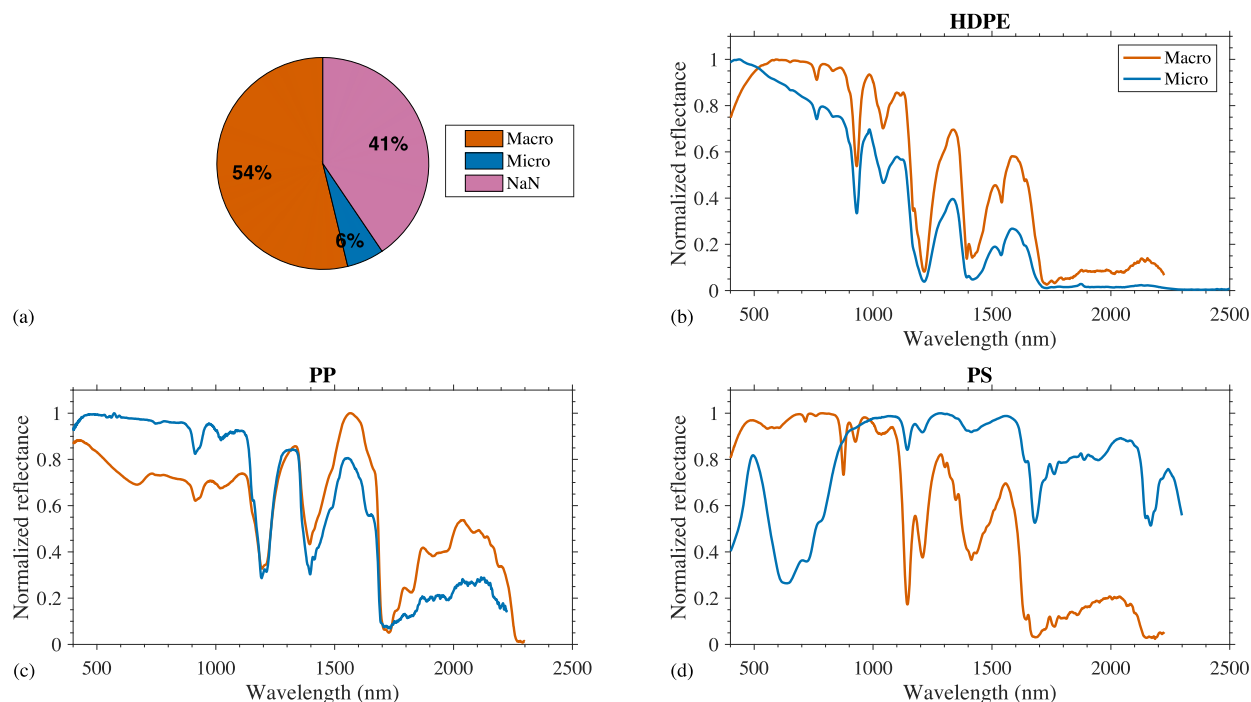
**Figure 8. (a) Categorical size distribution of samples within MADLib; and (b-d) example reflectance spectra of micro- and macro-sized (b) HDPE (c) PP, and (d) PS. Each reflectance spectrum was normalized to its own maximum reflectance value.**

**3.5 Weathering state**

The three categories of weathering - pristine, lab weathered and naturally weathered - have relatively equal contributions to the curated dataset, with less than one percent of samples left undefined (**Figure 9a**).

Case studies of three polymer types (PP, HDPE, and PA6) are presented before and after lab weathering (**Figure 9b-d**). Naturally weathered samples are not compared in the case study because no samples were measured before and after natural weathering for comparison. The two types of lab weathering, biofouling and UV exposure, produce different effects on reflectance within the visible spectrum. Samples exposed to UV radiation (dotted orange line) follow similar trends to their pristine counterparts with elevated reflectance values within the 1200-1600 nm range **(Figure 9b).** In comparison, all biofouled samples (solid orange lines) show reduced reflectance across the visible spectrum and exhibit a pronounced chlorophyll-a absorption feature at 670 nm (de Vries et al., 2023a) (**Figure 9b–d**). No major differences are found on the spectral shape in the NIR-SWIR region before and after biofouling; all the major spectral features for each polymer type remain the same.
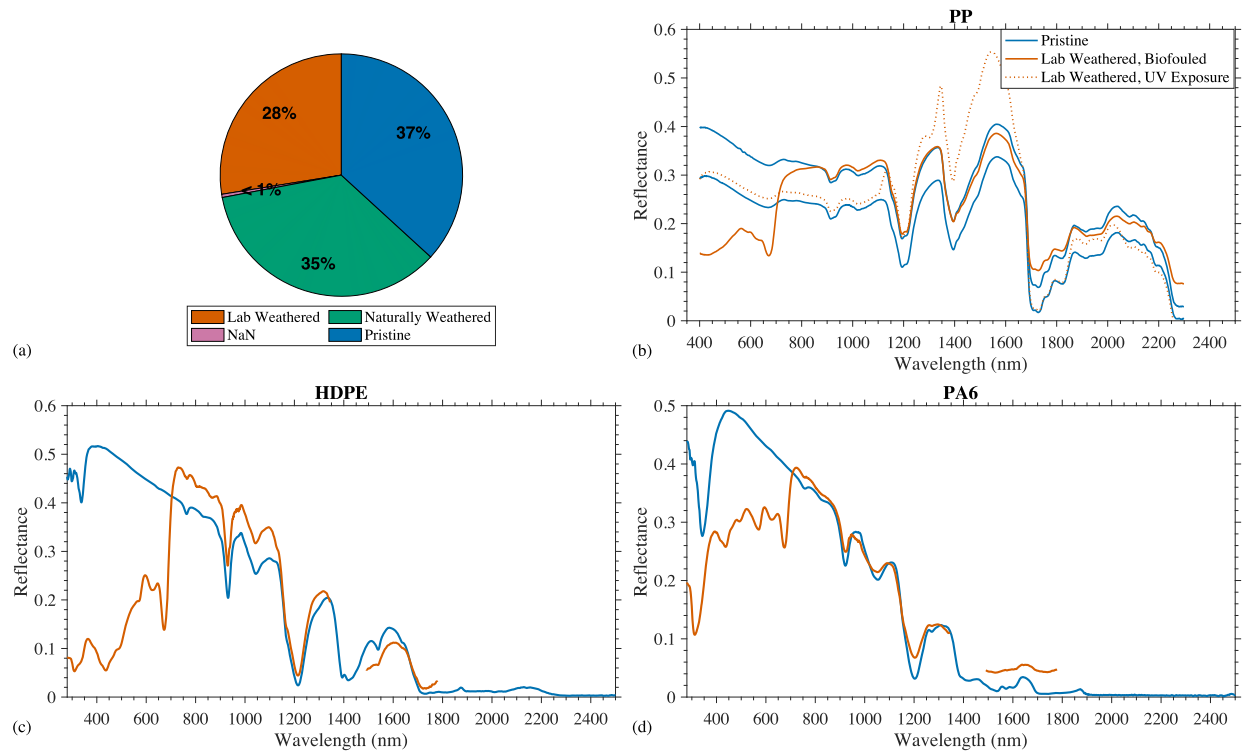
**Figure 9. (a) Distribution of weathering state categories within MADLib; and (b-d) example reflectance spectra for pristine and lab-weathered (biofouled or UV-exposed) samples: (b) PP, (c) HDPE, and (d) PA6.**

### 3.6 Aqueous state

In MADLib, submerged samples constitute the largest aqueous state category (43 %), followed by dry samples (35 %), with fewer classified as floating (14 %) or wet (8 %) (**Figure 10a)**. Each submerged object was measured at 3-20 separate depths to assess the effect of depth on spectral features, influencing the overall distribution. Less than one percent of samples is missing an aqueous state classification.

To examine the effect of the aqueous state on reflectance, a case study on the mean reflectance of pristine polypropylene samples from several datasets is presented. Reflectance magnitude decreases with increasing water interference in all cases, being highest for dry samples, followed by wet and floating/submerged samples. The case study reveals consistent spectral features in dry polypropylene across all four datasets (**Figure 10b-e**). The same spectral features are present for wet polypropylene samples as well (**Figure 10e-f**), but not present in submerged samples (**Figure 10c, e, f**). All submerged samples lose signal in the SWIR and their reflectance magnitudes decrease as depth increases (**Figure A1)**, both of which are expected due to water's high absorption in the IR (Garaba and Dierssen, 2020). Submerged samples exhibit unique peaks at approximately 810 and 1070 nm, which are consistent across datasets (**Figure 10c, e, f**) and polymer types (**Figure A1**). The floating objects represented from datasets 1 and 5 have pixel coverages of 66% and 60%, respectively, representing the highest available pixel coverage for dataset 1 and the closest match for dataset 5 (**Figure 10b, d**). The dataset 1 sample exhibits the same prominent SWIR absorption features when dry and wet, while the reflectance shape of the dataset 5 floating sample more closely resembles a submerged debris item (**Figure A2)**. The reflectance shape in the visible region is related to object color

322 in both cases. Both floating measurements have more noise and missing values in the infrared than the dry

323 measurements.
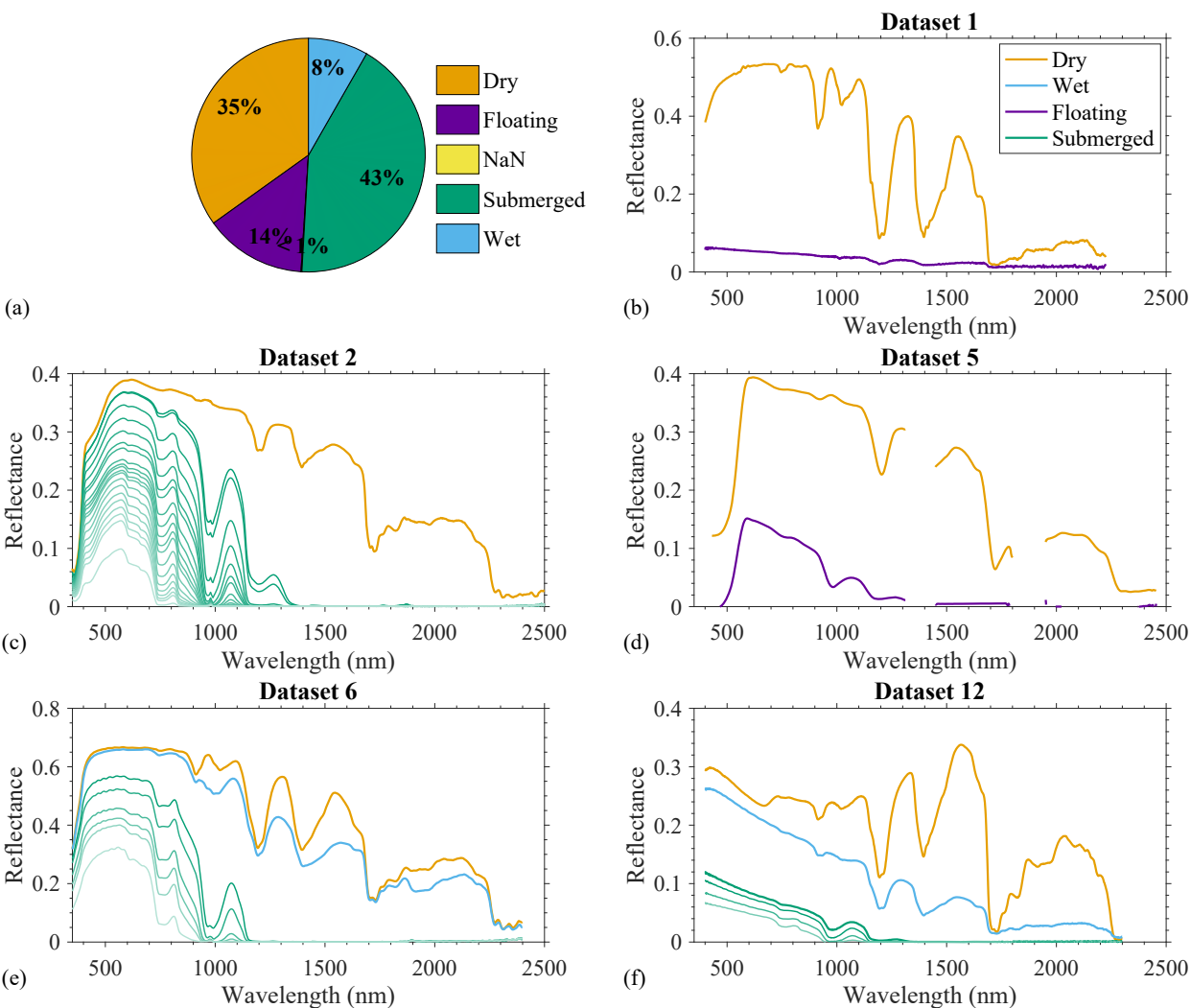
324
325 **Figure 10. (a) Distribution of aqueous state categories within MADLib; and (b-d) example reflectance spectra of dry**
326 **polypropylene across four aqueous state categories, using datasets (b) 1 (dry and floating), (c) 2 (dry and submerged), (d) 5**
327 **(dry and floating), (e) 6 (dry, wet, and floating), and (f) 12 (dry, wet, and floating). Submerged samples (c, e, f) are shown**
328 **at depths ranging from 5 to 715 mm.**

329 **4. Discussion**

330 The analysis of MADLib revealed distinct spectral features linked to various characteristics of debris, as well as key

331 gaps in available data. Below, we interpret these findings, highlight MADLib's utility and limitations, and offer

332 recommendations for future data collection and research directions.

333 **4.1 Preliminary lessons from MADLib**

334 MADLib offers a valuable and improved starting point for the development of algorithms aimed at detecting marine

335 debris, particularly plastics. Preliminary analyses highlight the role of apparent color and biofilm presence on spectral

shape in the visible spectrum (**Figure 7b, 9b**), whereas polymer type and aqueous state more strongly affect spectral shape in the SWIR region (**Figure 5b, 10b-f**). Previous studies have also found apparent color to influence spectral shape and magnitude in the visible spectrum, while the SWIR region remains largely unaffected regardless of the intrinsic color of the object (Knaeps et al., 2021; Garaba et al., 2021a). Biofouling of plastics has similar results, with the SWIR properties remaining largely unchanged, while spectral shape and magnitude are altered in the visible spectrum exhibiting a pronounced red edge feature (de Vries et al., 2023a). Measurements of wet, floating, and submerged debris show reduction in magnitude across the spectrum, especially in the SWIR, compared to dry debris (Knaeps et al., 2021; Garaba et al., 2021a; de Vries et al., 2023a). Submerged objects have minimal signal in the NIR-SWIR compared other aqueous states and unique spectral features in the NIR near 810 and 1070 nm (Knaeps et al., 2021; de Vries et al., 2023a). Distinct spectral differences between submerged plastics and other aqueous states (**Figure 10c, e, f**) suggest that separate detection algorithms may be required for submerged debris using the visible or NIR spectral regions. Given the limited polymer-specific features within the visible range, we further recommend focusing on SWIR wavelengths for algorithm development of non-submerged debris as prior studies have suggested (Garaba and Harmel, 2022). Several studies have demonstrated prospective plastic detection using high-resolution sensors with appropriate SWIR spectral bands (Guo and Li, 2020; Asadzadeh and Filho, 2016; Park et al., 2021; Kremezi et al., 2021), suggesting that prioritizing future sensors with appropriate spatial resolution (e.g. 30 m or less) and band placement can make SWIR-based approaches viable.

Although MADLib includes many samples categorized under the same polymer type and aqueous state, no two samples are identical. Every sample differs by at least one physical property or measurement condition, creating both challenges and opportunities. On one hand, polymer type comparisons (e.g., among polypropylene samples) may be confounded by variation within other sample characteristics, environmental perturbations, or experimental design (**Figure 5c, d**). On the other hand, this heterogeneity mirrors real-world conditions and provides a chance to identify robust spectral features that persist across variability. In this way, the breadth of measurement conditions available in MADLib can serve as a testing ground for existing plastic detection algorithms (Asadzadeh and Filho, 2017; Kühn et al., 2004; Zhang et al., 2022; Guo and Li, 2020; Garaba and Dierssen, 2018) and to derive general plastic endmember spectra (Hu, 2025). Beyond general plastic detection, it also provides opportunities for developing new approaches, including testing the feasibility of polymer-specific identification algorithms (Castagna et al., 2023; Moroni et al., 2015; Masoumi et al., 2012; Huth-Fehre et al., 1995). Detection of specific polymer types would aid in cleanup initiatives, polluter accountability, and policy development (NASEM, 2021).

**4.2 Considerations for future work**

MADLib would benefit from more complete metadata and greater representation of common debris types to increase its utility, as missing or inconsistent metadata currently hinders algorithm development. For example, the reflectance spectrum of a plastic object (e.g., a dry cup) offers limited insight if essential metadata like polymer type, color, or experimental design are missing. Many published datasets included in MADLib exhibited this issue. To address this, we propose a comprehensive metadata structure (**Table B1**) for future marine debris reflectance studies. We sorted

potential metadata into "required", "best practice", and "as needed" categories, acknowledging that some metadata maybe be difficult to obtain or unnecessary for future studies. **Table B2** summarizes the proposed changes to existing parameters (color and size) and introduces three new parameters (object ID, additives, and degree of weathering).

Future additions to MADLib should prioritize providing data on debris types that are currently underrepresented within the collection. For example, polymers such as PS, PE, and PPA along with colors like yellow, green, brown, and red have been recorded in marine debris surveys (Mutuku et al., 2024; Martí et al., 2020) but are poorly documented in MADLib (**Figure 5a, 7a**). Furthermore, floating samples were rarely included in MADLib (**Figure 10a**) yet they are the most detectable type of marine debris via remote sensing, warranting their characterization in future efforts. In addition, differences in the slopes of spectral features among samples of the same polymer type highlight the need for further investigation into the causes of such variability (**Figure 5c-d**). Differences in manufacturing processes, the presence of additives, and variations in experimental design are all potential factors that could contribute to these discrepancies. Future work should examine the effects of additives and other manufacturing treatments within the same polymer type, as these may influence optical properties and, by extension, detection and classification accuracy.

While our initiative focused on reflectance, the most widely available optical parameter, future curation efforts that incorporate additional optical properties will expand the applicability of MADLib across a broader range of sensors, including active systems (Palombi and Raimondi, 2022; Goddijn-Murphy et al., 2024; Behrenfeld et al., 2023; de Fockert et al., 2024).

MADLib also paves the way for collaborations among remote sensing scientists, modelers, and marine policy experts. The current dataset may also support mapping debris movement and, when combined with physical transport models e.g., (Maximenko and Hafner, 2024), can be used to forecast debris pathways to inform cleanup efforts and promote polluter accountability. Lastly, we would like to emphasize the need for open-science and open-access approaches to move this effort forward.

**5. Data availability**

MADLib is available in open access via https://doi.org/10.4121/059551d3-2383-4e20-af2d-011c9a59d3ac (Ohall et al., 2025). Two CSV files are included with the MADLib download: a metadata sheet and a data sheet. The samples can be linked across the two files using the *dataset number* and *sample number* columns.

**6. Conclusions**

MADLib represents a foundational step toward harmonizing spectral reflectance measurements for marine debris and is aligned with open-science policies. An important feature of the established MADLib collection is the traceable curation that allows ingestion of data from any permanent repository, dataset or reference library (e.g., Ocean Scan, PANGAEA, SeaBASS, SPECCHIO, USGS Spectral Library). We envision MADLib as a living resource where new

datasets can be added to maximize interoperability and findability of the collection. We believe that prioritizing the measurements and metadata gaps discussed in future research will strengthen MADLib as a remote sensing community resource. With its currently available data, and future iterations, MADLib will further support algorithm development and help establish important specifications for debris detection to be implemented in future remote sensing technologies.

**Appendix A**
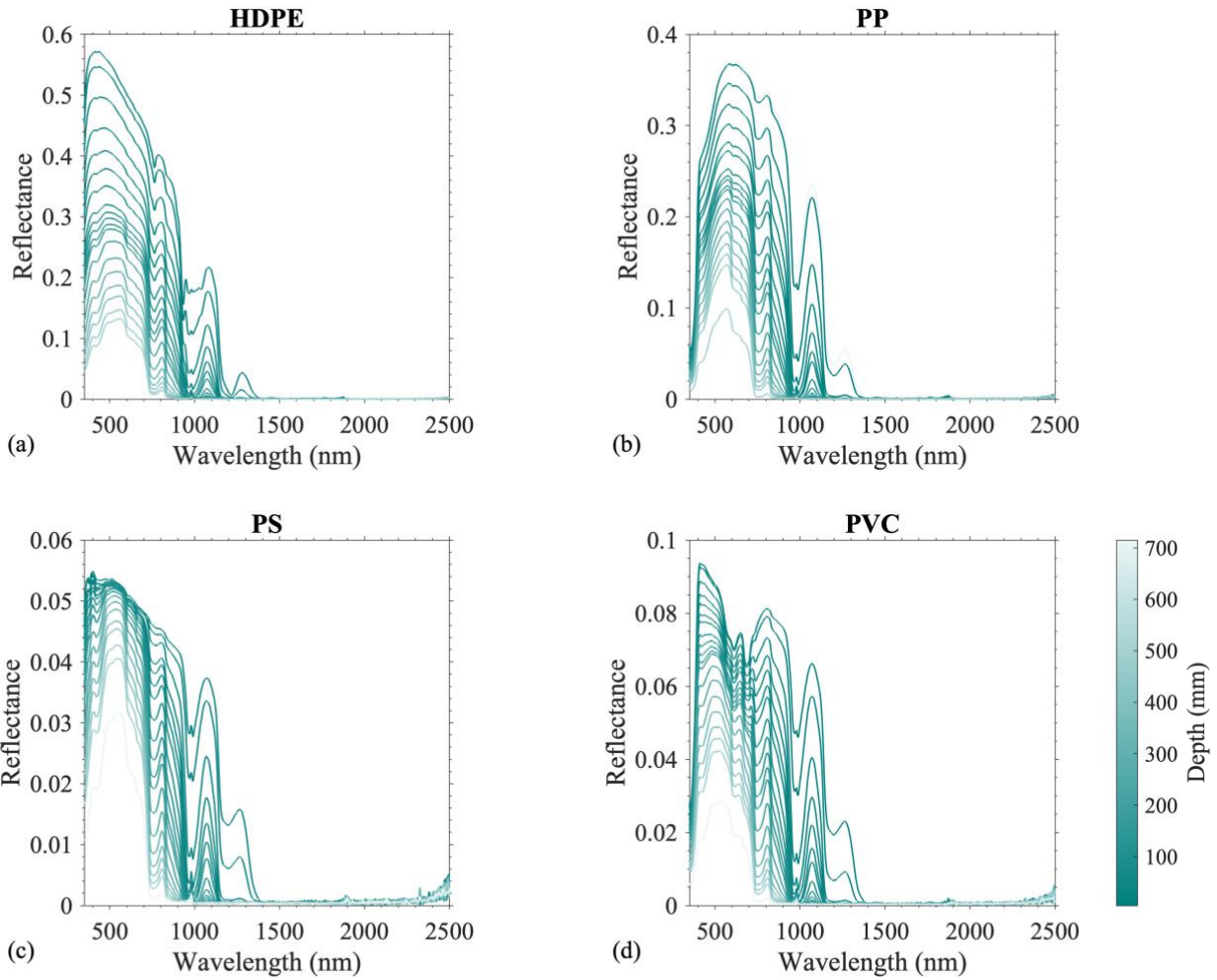
**Figure A1. Mean reflectance spectra of four polymer types – HDPE, PP, PS, and PVC - submerged to depths between 5-715 mm.**

412
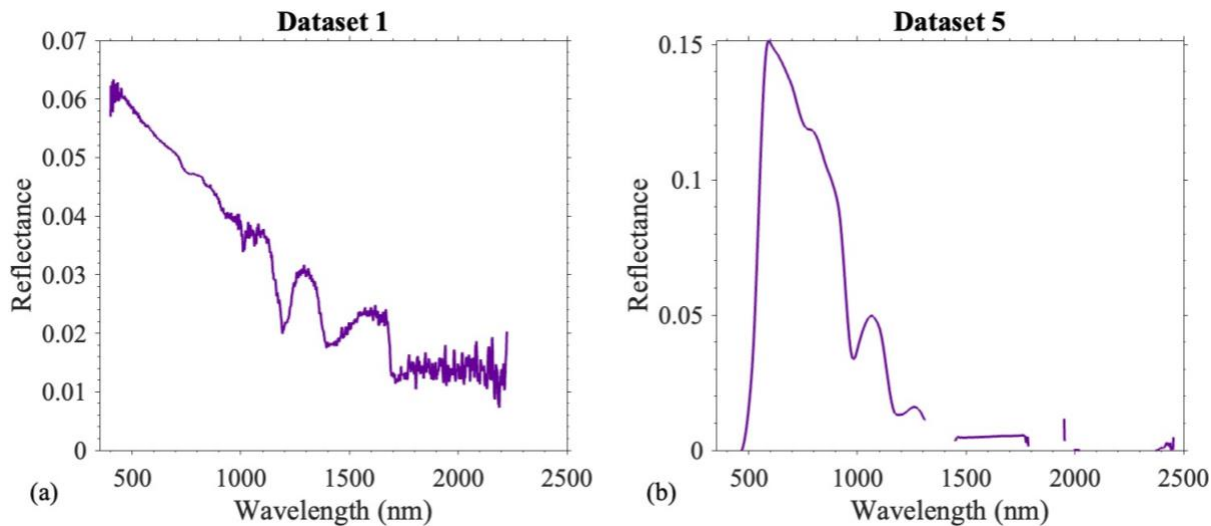
413    **Figure A2. Isolated reflectance spectra of floating samples from Figures 10b and 10d.**

414    **Appendix B**

415    **Table B1. Recommended metadata for future datasets, with required, best practice, and as needed metadata. See Table 2**
416    **for descriptions of metadata parameters.**

| Required | Best Practice | Optional |
|---|---|---|
| Object ID | Polymer Type | Lab Weathering Type |
| Object Type | Additives | Degree of weathering |
| Object State | | Submergence Depth (mm) |
| Origin | | Water Type |
| Color | | TSM (mg/L) |
| Categorical Size | | Algal Cell Density (cells/mL) |
| Weathering State | | Pixel Coverage (%) |
| Aqueous State | | Other |
| Instrument | | |
| Setting | | |
| Lighting | | |
| Background | | |
| Reference Standard | | |

| | | |
|---|---|---|
| Fixed Height from Sample (m) | | |
| FoV (deg) | | |
| Viewing Geometry (deg) | | |

417

418 **Table B2. Recommended improvements for future metadata collection of specific descriptors.**

| Descriptor | Structure in MADLib | Proposed metadata information |
|---|---|---|
| **Color** | Uses "Multi" for objects with multiple colors as described by original authors | Instead of using "Multi," list each observed color to improve interpretation of reflectance in the visible spectrum |
| **Size** | Provides both categorical (e.g., micro, macro) and dimensional (length, width, height) information | Categorical labels are sufficient if consistent cutoffs are applied (e.g., micro < 5 mm; macro ≥ 5 mm), as size had minimal impact on spectral feature locations (**Figure 5b**) |
| **Object ID** | Not currently included | Add to identify the same object measured under different conditions (e.g., dry vs. submerged) |
| **Additives** | Not currently included | For best practice, identify any additives |
| **Degree of weathering** | Not currently included | If the object is weathered, provide a metric for the degree of weathering |

419

420 **Author contribution**

421 Conceptualization: AO, KB, SPG; Data curation: AO; Formal Analysis: AO; Supervision: KB, SPG, SRC; Funding
422 Acquisition: KB, SRC; Writing – original draft preparation: AO; Writing- Review and Editing: SG, KB, SRC. All the
423 authors reviewed and approved the manuscript text.

424 **Competing Interests**

425 The authors declare that they have no conflict of interest.

426 **Acknowledgements**

427 The study was supported as part of a summer internship by AO at Science Mission Directorate at the National
428 Aeronautics and Space Administration headquarters. We appreciate the feedback on the study from members of
429 Rivero-Calle laboratory, Jay Brandes and Daniel Koestner. We thank Lee Ann Deleo for her help with Figure 1. The

430 authors are also grateful for the open-access and willingness to share data by the teams in table 1, without which this
431 work would not be possible.

**Financial Support**

433 AO was supported by the University of Georgia Graduate Tuition Return Incentive Program (GTRIP, 2023-2025) and
434 2024 National Aeronautics and Space Administration Headquarters summer internship reference code – 016758. SPG
435 was supported through Deutsche Forschungsgemeinschaft (DFG, German Research Foundation) – Projektnummer
436 417276871 and Basic Activities contract no. 4000132037/20/NL/GLC within the Discovery Element of the European
437 Space Agency.

**References**

439 Acuña-Ruz, T. and Mattar, C. B.: Thermal infrared spectral database of marine litter debris in Archipelago of Chiloé,
440 Chile, PANGAEA [dataset], https://doi.org/10.1016/j.rse.2018.08.008, 2020.

441 Asadzadeh, S. and Filho, C. R. d. S.: Investigating the capability of WorldView-3 superspectral data for direct
442 hydrocarbon detection, Remote Sensing of Environment, 173, https://doi.org/10.1016/j.rse.2015.11.030, 2016.

443 Asadzadeh, S. and Filho, C. R. d. S.: Spectral remote sensing for onshore seepage characterization: A critical overview,
444 Earth-Science Reviews, 168, https://doi.org/10.1016/j.earscirev.2017.03.004, 2017.

445 Beaumont, N. J., Aanesen, M., Austen, M. C., Börger, T., Clark, J. R., Cole, M., Hooper, T., Lindeque, P. K., Pascoe,
446 C., and Wyles, K. J.: Global ecological, social and economic impacts of marine plastic, Marine Pollution Bulletin,
447 142, https://doi.org/10.1016/j.marpolbul.2019.03.022, 2019.

448 Behrenfeld, M. J., Lorenzoni, L., Hu, Y., Bisson, K. M., Hostetler, C. A., Girolamo, P. D., Dionisi, D., Longo, F., and
449 Zoffoli, S.: Satellite Lidar Measurements as a Critical New Global Ocean Climate Record, Remote Sensing 2023, Vol.
450 15, Page 5567, 15, https://doi.org/10.3390/rs15235567, 2023.

451 Castagna, A., Dierssen, H. M., Devriese, L. I., Everaert, G., Knaeps, E., and Sterckx, S.: Evaluation of historic and
452 new detection algorithms for different types of plastics over land and water from hyperspectral data and imagery,
453 Remote Sensing of Environment, 298, https://doi.org/10.1016/j.rse.2023.113834, 2023.

454 Cheshire, A. C., Adler, E., Barbière, J., Cohen, Y., Evans, S., Jarayabhand, S., Jeftic, L., Jung, R. T., Kinsey, S., Kusui,
455 E. T., Lavine, I., Manyara, P., Oosterbaan, L., Pereira, M. A., Sheavly, S., Tkalin, A., Varadarajan, S., Wenneker, B.,
456 and Westphalen, G.: UNEP/IOC Guidelines on Survey and Monitoring of Marine Litter, UNEP and IOC, UNEP
457 Regional Seas Reports and Studies, No. 186; IOC Technical Series No. 83, xii + 120 pp.,
458 https://www.unep.org/resources/report/unepioc-guidelines-survey-and-monitoring-marine-litter, 2009.

Clark, R. N., Swayze, G. A., Livo, K. E., Kokaly, R. F., Sutley, S. J., Dalton, J. B., McDougal, R. R., and Gent, C. A.: Imaging spectroscopy: Earth and planetary remote sensing with the USGS Tetracorder and expert systems, Journal of Geophysical Research: Planets, 108, https://doi.org/10.1029/2002JE001847, 2003.

Corbari, L., Minacapilli, M., Ciraolo, G., and Capodici, F.: Indoor laboratory experiments for beach litter spectroradiometric analyses, Scientific Reports 2024 14:1, 14, https://doi.org/10.1038/s41598-024-74278-8, 2024.

Corbari, L., Maltese, A., Capodici, F., Mangano, M. C., Sarà, G., and Ciraolo, G.: Indoor spectroradiometric characterization of plastic litters commonly polluting the Mediterranean Sea: toward the application of multispectral imagery, Scientific Reports 2020 10:1, 10, https://doi.org/10.1038/s41598-020-74543-6, 2020.

de Fockert, A., Eleveld, M. A., Bakker, W., Felício, J. M., Costa, T. S., Vala, M., Marques, P., Leonor, N., Moreira, A., Costa, J. R., Caldeirinha, R. F. S., Matos, S. A., Fernandes, C. A., Fonseca, N., Simpson, M. D., Marino, A., Gandini, E., Camps, A., Perez-Portero, A., Gonga, A., Burggraaff, O., Garaba, S. P., Salama, M. S., Xiao, Q., Calvert, R., van den Bremer, T. S., and de Maagt, P.: Assessing the detection of floating plastic litter with advanced remote sensing technologies in a hydrodynamic test facility, Scientific Reports 2024 14:1, 14, https://doi.org/10.1038/s41598-024-74332-5, 2024.

de Vries, R. V. F. and Garaba, S. P.: Dataset of spectral reflectances and hypercubes of submerged plastic litter, including COVID-19 medical waste, pristine plastics, and ocean-harvested plastics, 4TU.ResearchData [dataset], https://doi.org/10.4121/769cc482-b104-4927-a94b-b16f6618c3b3.v1, 2023.

de Vries, R. V. F., Garaba, S. P., and Royer, S.-J.: Hyperspectral reflectance of pristine, ocean weathered and biofouled plastics from a dry to wet and submerged state, Earth System Science Data, 15, https://doi.org/10.5194/essd-15-5575-2023, 2023a.

de Vries, R. V. F., Garaba, S. P., and Royer, S.-J.: Dataset of spectral reflectances and hypercubes of submerged biofouled, pristine, and ocean-harvested marine litter, 4TU.ResearchData. [dataset], https://doi.org/10.4121/7c53b72a-be97-478b-9288-ff9c850de64b.v1, 2023b.

English, D. C. and Hu, C.: Field and laboratory measured floating matter reflectance initial results, EcoSIS [dataset], https://doi.org/10.21232/NxTTJsta, 2020.

Galgani, F., Maes, T., and Li, D.: Plastic and oceans, Analysis of Microplastics and Nanoplastics, https://doi.org/10.1016/B978-0-443-15779-0.00004-3, 2025.

Garaba, S. P. and Dierssen, H. M.: Spectral reference library of 11 types of virgin plastic pellets common in marine plastic debris, EcoSIS [dataset], https://doi.org/10.21232/C27H34, 2017.

488     Garaba, S. P. and Dierssen, H. M.: An airborne remote sensing case study of synthetic hydrocarbon detection using
489     short wave infrared absorption features identified from marine-harvested macro- and microplastics, Remote Sensing
490     of Environment, 205, https://doi.org/10.1016/j.rse.2017.11.023, 2018.

491     Garaba, S. P. and Dierssen, H. M.: Spectral reflectance of dry marine-harvested microplastics from North Atlantic and
492     Pacific Ocean., EcoSIS [dataset], https://doi.org/10.21232/jyxq-1m66, 2019a.

493     Garaba, S. P. and Dierssen, H. M.: Spectral reflectance of washed ashore macroplastics., EcoSIS [dataset],
494     https://doi.org/10.21232/ex5j-0z25, 2019b.

495     Garaba, S. P. and Dierssen, H. M.: Spectral reflectance of dry and wet marine-harvested microplastics from Kamilo
496     Point, Pacific Ocean., EcoSIS [dataset], https://doi.org/10.21232/r7gg-yv83, 2019c.

497     Garaba, S. P. and Dierssen, H. M.: Hyperspectral ultraviolet to shortwave infrared characteristics of marine-harvested,
498     washed-ashore and virgin plastics, Earth System Science Data, 12, https://doi.org/10.5194/essd-12-77-2020, 2020.

499     Garaba, S. P. and Harmel, T.: Top-of-atmosphere hyper and multispectral signatures of submerged plastic litter with
500     changing water clarity and depth, Optics Express, Vol. 30, Issue 10, pp. 16553-16571, 30,
501     https://doi.org/10.1364/OE.451415, 2022.

502     Garaba, S. P., Acuña-Ruz, T., and Mattar, C. B.: Hyperspectral longwave infrared reflectance spectra of naturally
503     dried algae, anthropogenic plastics, sands and shells, Earth System Science Data, 12, 10.5194/essd-12-2665-2020,
504     2020a.

505     Garaba, S. P., de Vries, R. V. F., Knaeps, E., Mijnendonckx, J., and Sterckx, S.: Spectral reflectance measurements
506     of dry and wet virgin plastics at varying water depth and water clarity from UV to SWIR (SEV-1), 4TU.ResearchData
507     [dataset], https://doi.org/10.4121/uuid:9ee3be54-9132-415a-aaf2-c7fbf32d2199, 2020b.

508     Garaba, S. P., Arias, M., Corradi, P., Harmel, T., Vries, R. d., and Lebreton, L.: Concentration, anisotropic and
509     apparent colour effects on optical reflectance properties of virgin and ocean-harvested plastics, Journal of Hazardous
510     Materials, 406, https://doi.org/10.1016/j.jhazmat.2020.124290, 2021a.

511     Garaba, S. P., Castagna, A., Devriese, L. I., Dierssen, H. M., Everaert, G., Knaeps, E., and Sterckx, S.: Spectral
512     reflectance measurements of dry and wet plastic materials, asphalt, concrete klinker from UV-350 nm to SWIR-2500
513     nm around Spuikom, Belgium, PANGAEA [dataset], https://doi.org/10.1594/PANGAEA.937185, 2021b.

514     Garaba, S. P., Albinus, M., Bonthond, G., Flöder, S., Miranda, M. L. M., Rohde, S., Yong, J. Y. L., and Wollschläger,
515     J.: Bio-optical properties of the cyanobacterium *Nodularia spumigena*, Earth System Science Data, 15,
516     https://doi.org/10.5194/essd-15-4163-2023, 2023.

517   GIZ: Advances in remote sensing of plastic waste, Giang, P. and Ortwig, N. (Eds.), Deutsche Gesellschaft für

518   Internationale Zusammenarbeit (GIZ) GmbH, 87 pp., https://www.giz.de/en/downloads/giz-2023-en-advances-in-

519   remote-sensing-of-plastic-waste.pdf, 2023.

520   Goddijn-Murphy, L., Martínez-Vicente, V., Dierssen, H. M., Raimondi, V., Gandini, E., Foster, R., and Chirayath,

521   V.: Emerging Technologies for Remote Sensing of Floating and Submerged Plastic Litter, Remote Sensing 2024, Vol.

522   16, Page 1770, 16, https://doi.org/10.3390/rs16101770, 2024.

523   Guo, X. and Li, P.: Mapping plastic materials in an urban area: Development of the normalized difference plastic

524   index using WorldView-3 superspectral data, ISPRS Journal of Photogrammetry and Remote Sensing, 169,

525   https://doi.org/10.1016/j.isprsjprs.2020.09.009, 2020.

526   Hu, C.: Remote detection of marine debris using satellite observations in the visible and near infrared spectral range:

527   Challenges and potentials, Remote Sensing of Environment, 259, https://doi.org/10.1016/j.rse.2021.112414, 2021.

528   Hu, C.: On the logic of remote detection of plastic litter in the aquatic environments: A revisit, Remote Sensing of

529   Environment, 329, https://doi.org/10.1016/j.rse.2025.114911, 2025.

530   Hu, C., Qi, L., English, D. C., Wang, M., Mikelsons, K., Barnes, B. B., Pawlik, M. M., and Ficek, D.: Pollen in the

531   Baltic Sea as viewed from space, Remote Sensing of Environment, 284, https://doi.org/10.1016/j.rse.2022.113337,

532   2023.

533   Huth-Fehre, T., Feldhoff, R., Kantimm, T., Quick, L., Winter, F., Cammann, K., Broek, W. v. d., Wienke, D., Melssen,

534   W., and Buydens, L.: NIR - Remote sensing and artificial neural networks for rapid identification of post consumer

535   plastics, Journal of Molecular Structure, 348, https://doi.org/10.1016/0022-2860(95)08609-Y, 1995.

536   Knaeps, E., Strackx, G., Meire, D., Sterckx, S., Mijnendonckx, J., and Moshtaghi, M.: Hyperspectral reflectance of

537   marine plastics in the VIS to SWIR (2), 4TU.ResearchData [dataset], https://doi.org/10.4121/12896312.v2, 2020.

538   Knaeps, E., Sterckx, S., Strackx, G., Mijnendonckx, J., Moshtaghi, M., Garaba, S. P., and Meire, D.: Hyperspectral-

539   reflectance dataset of dry, wet and submerged marine litter, Earth System Science Data, 13,

540   https://doi.org/10.5194/essd-13-713-2021, 2021.

541   Kremezi, M., Kristollari, V., Karathanassi, V., Topouzelis, K., Kolokoussis, P., Taggio, N., Aiello, A., Ceriola, G.,

542   Barbone, E., and Corradi, P.: Pansharpening PRISMA Data for Marine Plastic Litter Detection Using Plastic Indexes

543   | IEEE Journals & Magazine | IEEE Xplore, IEEE Access, 9, https://doi.org/10.1109/ACCESS.2021.3073903, 2021.

544   Kühn, F., Oppermann, K., and Hörig, B.: Hydrocarbon Index – an algorithm for hyperspectral detection of

545   hydrocarbons, International Journal of Remote Sensing, 25, https://doi.org/10.1080/01431160310001642287, 2004.

546 Leone, G., Catarino, A. I., De Keukelaere, L., Bossaer, M., Knaeps, E., and Everaert, G.: Hyperspectral reflectance
547 dataset for dry, wet and submerged plastics in clear and turbid water, Marine Data Archive [dataset],
548 https://doi.org/10.14284/530, 2021.

549 Leone, G., Catarino, A. I., De Keukelaere, L., Bossaer, M., Knaeps, E., and Everaert, G.: Hyperspectral reflectance
550 dataset of pristine, weathered, and biofouled plastics, Earth System Science Data, 15, https://doi.org/10.5194/essd-15-
551 745-2023, 2023.

552 Martí, E., Martin, C., Galli, M., Echevarría, F., Duarte, C. M., and Cózar, A.: The Colors of the Ocean Plastics,
553 Environmental Science & Technology, 54, https://doi.org/10.1021/acs.est.9b06400, 2020.

554 Martínez-Vicente, V., Clark, J. R., Corradi, P., Aliani, S., Arias, M., Bochow, M., Bonnery, G., Cole, M., Cózar, A.,
555 Donnelly, R., Echevarría, F., Galgani, F., Garaba, S. P., Goddijn-Murphy, L., Lebreton, L., Leslie, H. A., Lindeque,
556 P. K., Maximenko, N., Martin-Lauzer, F.-R., Moller, D., Murphy, P., Palombi, L., Raimondi, V., Reisser, J., Romero,
557 L., Simis, S. G. H., Sterckx, S., Thompson, R. C., Topouzelis, K. N., Sebille, E. v., Veiga, J. M., and Vethaak, A. D.:
558 Measuring Marine Plastic Debris from Space: Initial Assessment of Observation Requirements, Remote Sensing 2019,
559 Vol. 11, Page 2443, 11, https://doi.org/10.3390/rs11202443, 2019.

560 Masoumi, H., Safavi, S. M., and Khani, Z.: Identification and classification of plastic resins using near infrared
561 reflectance, Int. J. Mech. Ind. Eng, 6, 213-220, 2012.

562 Maximenko, N. and Hafner, J.: Near-real time model product to support marine debris research and operations in
563 Hawaii and in the eastern North Pacific, International Pacific Research Center, IPRC Technical Note No. 7, , 17 pp.,
564 https://iprc.soest.hawaii.edu/publications/tech_notes/NPac-GP-TechNote-7.pdf, 2024.

565 Maximenko, N., Corradi, P., Law, K. L., Van Sebille, E., Garaba, S. P., Lampitt, R. S., Galgani, F., Martinez-Vicente,
566 V., Goddijn-Murphy, L., Veiga, J. M., Thompson, R. C., Maes, C., Moller, D., Löscher, C. R., Addamo, A. M.,
567 Lamson, M. R., Centurioni, L. R., Posth, N. R., Lumpkin, R., Vinci, M., Martins, A. M., Pieper, C. D., Isobe, A.,
568 Hanke, G., Edwards, M., Chubarenko, I. P., Rodriguez, E., Aliani, S., Arias, M., Asner, G. P., Brosich, A., Carlton, J.
569 T., Chao, Y., Cook, A.-M., Cundy, A. B., Galloway, T. S., Giorgetti, A., Goni, G. J., Guichoux, Y., Haram, L. E.,
570 Hardesty, B. D., Holdsworth, N., Lebreton, L., Leslie, H. A., Macadam-Somer, I., Mace, T., Manuel, M., Marsh, R.,
571 Martinez, E., Mayor, D. J., Le Moigne, M., Molina Jack, M. E., Mowlem, M. C., Obbard, R. W., Pabortsava, K.,
572 Robberson, B., Rotaru, A.-E., Ruiz, G. M., Spedicato, M. T., Thiel, M., Turra, A., and Wilcox, C.: Frontiers | Toward
573 the Integrated Marine Debris Observing System, Frontiers in Marine Science, 6,
574 https://doi.org/10.3389/fmars.2019.00447, 2019.

575 Moroni, M., Mei, A., Leonardi, A., Lupo, E., and Marca, F. L.: PET and PVC Separation with Hyperspectral Imagery,
576 Sensors 2015, Vol. 15, Pages 2205-2227, 15, https://doi.org/10.3390/s150102205, 2015.

577    Mutuku, J., Yanotti, M., Tocock, M., and MacDonald, D. H.: The Abundance of Microplastics in the World's Oceans:

578    A Systematic Review, Oceans 2024, Vol. 5, Pages 398-428, 5, https://doi.org/10.3390/oceans5030024, 2024.

579    NASEM: Reckoning with the U.S. Role in Global Ocean Plastic Waste, The National Academies of Sciences,

580    Engineering, and Medicine, Washington, DC978-0-309-45885-6, 269 pp., https://doi.org/10.17226/26132, 2021.

581    Ohall, A., Bisson, K., and Rivero-Calle, S.: MArine Debris hyperspectral reference Library collection (MADLib),

582    4TU.ResearchData [dataset], https://doi.org/10.4121/059551d3-2383-4e20-af2d-011c9a59d3ac, 2025.

583    Olyaei, M., Ebtehaj, A., and Ellis, C. R.: A Hyperspectral Reflectance Database of Plastic Debris with Different

584    Fractional Abundance in River Systems, Scientific Data 2024 11:1, 11, https://doi.org/10.1038/s41597-024-03974-x,

585    2024.

586    Palombi, L. and Raimondi, V.: Experimental Tests for Fluorescence LIDAR Remote Sensing of Submerged Plastic

587    Marine Litter, Remote Sensing 2022, Vol. 14, Page 5914, 14, https://doi.org/10.3390/rs14235914, 2022.

588    Park, Y.-J., Sainte-Rose, B., and Garaba, S. P.: Detecting the Great Pacific Garbage Patch floating plastic litter using

589    WorldView-3 satellite imagery, Optics Express, Vol. 29, Issue 22, pp. 35288-35298, 29,

590    https://doi.org/10.1364/OE.440380, 2021.

591    Smith, G. and Garaba, S. P.: Insights from monitoring abundances and characteristics of plastic leakage in city

592    waterways and tourist beaches of Cambodia, Environmental Challenges, 19,

593    https://doi.org/10.1016/j.envc.2025.101121, 2025.

594    Tasseron, P., Emmerik, T. v., Peller, J., Schreyers, L., and Biermann, L.: Advancing Floating Macroplastic Detection

595    from Space Using Experimental Hyperspectral Imagery, Remote Sensing 2021, Vol. 13, Page 2335, 13,

596    https://doi.org/10.3390/rs13122335, 2021.

597    Thompson, R. C., Courtene-Jones, W., Boucher, J., Pahl, S., Raubenheimer, K., and Koelmans, A. A.: Twenty years

598    of microplastic pollution research—what have we learned?, Science, 386, https://doi.org/10.1126/science.adl2746,

599    2024.

600    UNEP: Drowning in Plastics – Marine Litter and Plastic Waste Vital Graphics, United Nations Environment

601    Programme (UNEP), Secretariats of the Basel, Rotterdam and Stockholm Conventions (BRS) and GRID-Arendal, 77

602    pp., https://wedocs.unep.org/xmlui/bitstream/handle/20.500.11822/36964/VITGRAPH.pdf, 2021.

603    Wang, S., Zhao, W., Sun, D., Li, Z., Shen, C., Bu, X., and Zhang, H.: Unveiling reflectance spectral characteristics of

604    floating plastics across varying coverages: insights and retrieval model, Optics Express, 32, 22078-22094,

605    https://doi.org/10.1364/OE.521004, 2024.

606 Wilkinson, M. D., Dumontier, M., Aalbersberg, I. J., Appleton, G., Axton, M., Baak, A., Blomberg, N., Boiten, J.-W.,

607 da Silva Santos, L. B., and Bourne, P. E.: The FAIR Guiding Principles for scientific data management and

608 stewardship, Scientific data, 3, 1-9, https://doi.org/10.1038/sdata.2016.18, 2016.

609 Zhang, P., Du, P., Guo, S., Zhang, W., Tang, P., Chen, J., and Zheng, H.: A novel index for robust and large-scale

610 mapping of plastic greenhouse from Sentinel-2 images, Remote Sensing of Environment, 276,

611 https://doi.org/10.1016/j.rse.2022.113042, 2022.

612